Journal of Quantitative Spectroscopy & Radiative Transfer 242 (2020) 106774

Contents lists available at ScienceDirect

Journal of Quantitative Spectroscopy & Radiative Transfer

journal homepage: www.elsevier.com/locate/jqsrt

Continuum absorption of millimeter waves in nitrogen

E.A. Serov[a,*], A.A. Balashov[a], M.Yu. Tretyakov[a], T.A. Odintsova[a], M.A. Koshelev[a], D.N. Chistikov[b,c], A.A. Finenko[b], S.E. Lokshtanov[c], S.V. Petrov[b], A.A. Vigasin[c]

[a] Institute of Applied Physics of the Russian Academy of Sciences, 46 Ulyanov str., Nizhny Novgorod 603950, Russia
[b] Department of Chemistry, Lomonosov Moscow State University, GSP-1, 1 Vorobievy Gory, Moscow 119991, Russia
[c] Obukhov Institute of Atmospheric Physics, Russian Academy of Sciences, 3 Pyzhevsky per., Moscow 119017, Russia

ARTICLE INFO

Article history:
Received 25 October 2019
Revised 21 November 2019
Accepted 21 November 2019
Available online 22 November 2019

Keywords:
Collision-induced absorption
Dry air continuum
Millimeter wavelength range

ABSTRACT

We report the results of experimental study for the N_2 absorption in the millimeter wavelength range at pressure and temperature ranging, respectively, from 750 to 1500 Torr and from 265 to 310 K. The obtained data are shown to be in a good agreement with the previously published experimental results, as well as with the predictions issued from available empirical models of nonresonant absorption and from the simulation of the N_2–N_2 rototranslational collision-induced absorption performed recently using the classical trajectories method relying on complete *ab initio* potential and induced dipole surfaces. Analysis of the first spectral moments leads to a conclusion that the role of true bound $(N_2)_2$ dimer absorption is negligible at least in the range of atmospheric temperatures. New experimental data reported in this paper are supported by our theoretical modelling being however somewhat in excess of the data presented in the HITRAN/CIA database for the same spectral range. We consider our data as an update of the previously available so-called "dry" atmospheric continuum which is conventionally employed nowadays in the mm-waves propagation models.

1. Introduction

The propagation of centimeter, millimeter and submillimeter waves in the Earths atmosphere has been a subject of research for many decades. The early measurements made by Becker and Autler [1] at atmospheric pressure showed that the entire observable absorption cannot be explained in terms of accumulated contribution of the atmospheric gases resonant lines broadened according to the conventional impact line shape theory. The absorption near the resonant line centers agrees well with predictions as far as the results of precise measurements of line frequency, line width and intensity are concerned. In contrast, in the intervals between the lines the absorption is much higher than the cumulative contribution from the lines calculated using the Van Vleck-Weisskopf individual line-shapes [2]. This excess absorption is usually called the continuum absorption or the continuum. It arises as a result of pairwise interaction between molecules. The spectra of dipoleless molecules do not exhibit resonant absorption lines in the millimeter and far infrared ranges, provided quadrupole or higher order absorption can be neglected. Hence, the entire observed absorption is caused by intermolecular interaction between non-polar partners of collisions. Intermolecular interaction induces a temporary weak dipole moment in molecular pairs which is responsible for the so-called collision-induced absorption (CIA). The probability of pair collisions is several orders in excess of triple collisions throughout the range of pressure and temperature typical for the Earths atmosphere. This means that the consideration of only pair collisions is justified for examination of radiation propagation through the atmosphere. The totality of molecular pairs in a gas at equilibrium can be divided into sub-groups called free pairs, quasi-bound (metastable) pairs and true bound dimers, depending on the domain in the phase space attributable to each of these categories [3–5].

The atmospheric continuum can be subdivided into dry air continuum dominated by nitrogen and the water vapor continuum. Their relative contributions vary significantly as a function of the height in the atmosphere as a result of the change in the altitude profile of humidity. In the near-surface lower troposphere under the summer temperate conditions the dry air continuum is approximately two orders of magnitude weaker than the water vapor continuum. However, at the altitude as high as ten kilometers or more than that, the water content in air becomes so low [6] that the magnitude of dry air continuum becomes significant or even dominant.

* Corresponding author.
E-mail address: serov@ipfran.ru (E.A. Serov).

https://doi.org/10.1016/j.jqsrt.2019.106774
0022-4073/

There are many publications that report results of laboratory and theoretical studies of continuum absorption, in particular, the dry air continuum in the millimeter and submillimeter spectral ranges. Several examples are worth mentioning, including investigations of the pressurized oxygen absorption [7,8], the high-pressure measurements of continuum absorption in nitrogen and in other gases [9]. To the best of our knowledge, the most recent work devoted to a detailed laboratory study of continuum absorption in dry atmospheric gases in the millimeter spectral range under nearly atmospheric conditions was published by Meshkov and De Lucia in 2007 [10]. In this paper the results of the investigation related to absorption in N_2, O_2 and in dry air at pressure ranging from one to three atmospheres within the temperature range from 230 to 320 K are reported.

Despite the significant progress reached in the recent years in understanding of the physical mechanisms responsible for the continuum, there exists no universal and feasible model that could permit unambiguous evaluation of this absorption for any molecular pairs. Therefore, empirical models are used to simulate propagation of radiation, provided the continuum must be taken into account. One of the widely used models of millimeter and submillimeter-wave propagation was developed by Liebe [11–13] and further upgraded by Rosenkranz [14,15]. The present day version of the Liebe-Rosenkranz model (Millimeter Wave Propagation Model, MPM for short) comprises a sum of lines, the parameters of which were measured in laboratory experiments or, in some cases, calculated theoretically, and also the continuum part determined semiempirically [15].

The need for more accurate than the present day knowledge of the microwave absorption in gases is associated with the growing demand for accuracy of the propagation model required for atmospheric parameters retrievals from remote sensing [16,17]. The millimeter-submillimeter range is used in the ground-based and satellite radiometry for the retrieval of temperature profiles, atmospheric humidity, and determination of the various impurities concentration [18–20].

It is believed (see, for example, the review articles [21,22]) that multiple measurements are needed for determining a reliable value of line parameters in different experimental conditions using spectrometers of different types. This refers to a greater extent to the continuum parameters, which are known with much lower accuracy than that typical for the resonant line parameters [17]. This is conditioned by complexity of laboratory measurements of the continuum specified by its low intensity under usual conditions and weak frequency dependence, which demands high sensitivity and stability of the parameters of experimental setup.

Besides remote sensing of the Earths atmosphere, precise continuum measurements are required for exploration of other planets and cosmic bodies such as exoplanets and satellites. In particular, investigation of the CIA spectrum of nitrogen is important for the simulation of radiative transfer in the Titans atmosphere consisting of approximately 95% of nitrogen, 5% of methane and other less represented constituents [23].

In view of a limited amount of available experimental data, new precise experimental studies of nitrogen continuum are in high demand. They could increase accuracy of the already available spectroscopic models as well as feed the upcoming continuum absorption theory with accurately measured reference characteristics. The results reported in the present work are related to the study of the nitrogen spectrum in the millimeter wavelength range at nearly atmospheric pressures and temperatures using a resonator spectrometer.

The experimental procedure is described in the Section 2. The experimental data processing and the analysis of the temperature and pressure dependence of the spectra are reported in Section 3. The classical trajectory method is briefly described in Section 4 along with the calculation of the spectral moments. In Section 5 the results of this work are discussed and compared with the previous experimental and theoretical data with critical evaluation of the available theoretical approaches. New values are recommended for parameters in the empirical model, intended for the calculation of atmospheric absorption based on consolidated experimental data.

2. Experiment

The measurements were performed on a resonator spectrometer [24,25], with a high-Q ($Q = f/\Delta f \approx 10^6$) Fabry-Perot resonator used as a sensing element. The absorption measurements are based on the change in the Q-factor of the resonator filled with absorbing gas. This change is assessed by measuring the width of the resonance curve. These widths (Δf_0) determining the intrinsic losses of radiation power in the resonator filled with a non-absorbing gas, including diffraction losses, coupling losses, and mirror reflection losses, are measured at the eigenfrequencies of the resonator modes. The widths (Δf) determining losses in a resonator filled with the gas under study are measured analogously. The loss of radiation power due to absorption in gas is defined as the difference between the measured losses. The absorption coefficient α for $\alpha L \ll 1$ (L is the resonator length) is calculated by the expression

$$\alpha = 2\pi(\Delta f - \Delta f_0)/c, \tag{1}$$

where c is the speed of light. Argon is used as a non-absorbing gas, with the pressure chosen such that its refractive index is equal to the refractive index of the studied gas. The optical path length is the same in both measurements and the intrinsic resonator losses and the losses of the resonator filled with the studied gas are measured at the same frequencies. The resonator is placed in a stainless steel chamber with a volume of approximately 200 liters coated on the outside with foam polyethylene for thermal insulation from the environment. The resonator temperature is kept constant by means of an active controlled thermostat (Julabo FP-5, the accuracy of setting coolant temperature is 0.01 °C). The coolant circulates over a copper tube attached to a thick-wall (5 mm) copper casing of the resonator. The temperature is controlled by platinum sensors (the uncertainty is 0.2 °C) placed on the resonator elements (casing and mirrors), as well as in free space. The temperature of the elements of the quasi-optical waveguide line is maintained constant during the experiment. This allows minimizing the influence of the parasitic reflections which interfere with useful signals and lead to the dependence of the measured values of Δf and Δf_0 on the length of the quasi-optical waveguide line [25]. Gas pressure is measured by means of two Baratron sensors having the range up to 1000 Torr and up to 2000 Torr and the declared relative error of 0.25%.

A backward wave oscillator (BWO) is used as a radiation source. Precision control and stabilization of the radiation frequency are provided by a phase-locked-loop (PLL) system. A detailed description of the spectrometer can be found in [25].

Before each gas inlet, the chamber was evacuated to a pressure of less than 5×10^{-3} Torr. As a rule, the chamber was first filled with nitrogen (volume fraction $N_2 \geq 99.999\%$), and then the absorption was measured with simultaneous recording of the pressure and temperature. After that nitrogen was pumped out and the chamber was filled with argon (volume fraction Ar $\geq 99.998\%$) for measuring the resonator intrinsic losses. After each gas inlet, its temperature was controlled until its difference from the preset value became an order of measurement uncertainty, which indicated that thermodynamic equilibrium with the internal parts of the chamber and the resonator casing was achieved. The duration of thermalization depended on the difference between the preset

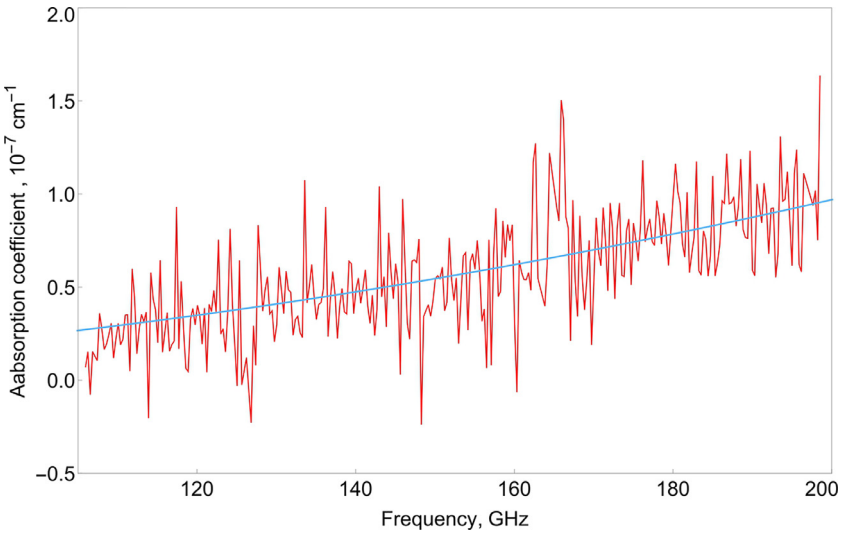

Fig. 1. Typical recording of nitrogen absorption spectrum (p =1000 Torr, T =288 K). Red line – experimental data, blue line – approximation by the function $y = a \cdot \nu^2$. (For interpretation of the references to colour in this figure legend, the reader is referred to the web version of this article.)

temperature of the gas and room temperature and, as a rule, did not exceed 20 min after which spectrum recording was started.

During spectrum recording that lasted for approximately 30 min the gas temperature varied within 0.2° C. However, the temperature stability of the resonator mirrors was worse, as during pumping out the gas from the chamber the heat exchange between the resonator and the environment decreased, which resulted in changes in the resonator temperature, whereas the temperature of the coolant remained constant. The value of intrinsic losses depends on the temperature of the resonator mirrors. Although the variations of mirror temperature during the experiment did not exceed 0.6 °C, the absorption in nitrogen was so weak that even such changes led to a significant (approximately 10% under our conditions) error in gas absorption measurements. The variation of mirror temperature was taken into consideration in the calculation of the intrinsic resonator losses using the data of the work [26].

Two different BWOs operating in the 105–150 GHz and 105–200 GHz ranges with slightly different configurations of quasi-optical waveguide lines were used for the measurements. More than 100 spectra at the pressures from 750 to 1500 Torr and temperatures from 265 to 310 K were recorded. An example of the spectrum recording is presented in Fig. 1. A large spread of points is due to the weak measured absorption, which is only 20 times more than the ultimate spectrometer sensitivity, even at a pressure of 2 atm.

Several recordings were made for each set of meteorological parameters (pressure, temperature). They differed in the displacement of the quasi-optical line relative to the resonator and the corresponding changes in the phase of the standing waves arising due to spurious reflections and contributing to the error. By averaging these recordings, 24 nitrogen spectra were obtained for 6 temperature points and 4 pressure points.

3. Processing of the experimental data

The continuum absorption spectra in pure gases in the millimeter range are usually analysed using the following empirical approximation:

$$\alpha^{N_2-N_2}(\nu, p, T) = k(p, T) \cdot \nu^2 \tag{2}$$

where:

$$k(p, T) = C(T) \cdot p^2, \tag{3}$$

$$C(T) = C_0 \cdot (T_0/T)^n \tag{4}$$

$\alpha^{N_2-N_2}$ is absorption coefficient, ν is radiation frequency, p is gas pressure, T is gas temperature, T_0 =300 K, and C_0 and n are fitting parameters.

This approximation neglects the features of the spectral function of bimolecular absorption due to which the absorption steadily deviates from the quadratic dependence as frequency increases [3]. Somewhat more accurate approximation having these features taken into account is used in the MPM [15]. The small correction used in the MPM allows applying it not only in the millimeter but also in the submillimeter range (up to about 2 THz):

$$\alpha_{MPM}^{N_2-N_2}(\nu, p, T) = k_M(p, T) \cdot \frac{\nu^2}{2} \cdot \left(1 + \frac{1}{(1+\nu/450)^2}\right) \tag{5}$$

where frequency ν is in GHz, $k_M(p, T) = C_M \cdot (T_0/T)^{n_M} \cdot p^2$, C_M and n_M are the fitting parameters the values of which for the MPM were obtained from quantum calculations of absorption in nitrogen [27]. The collision-induced absorption in dry air is determined based on the fact that at frequencies up to 3 THz it is directly proportional to the absorption in nitrogen under the same conditions [28]. The coefficient of proportionality between the corresponding parameters C_0 in air and in nitrogen (Eq. (4)) is 0.84. Making use of this ratio we can find parameters of the present day version of the MPM for nitrogen: $C_M = 1.85 \times 10^{-18}$ $cm^{-1}/(Torr\ GHz)^2$, and $n_M = 3.6$.

The difference between the results of approximation of the obtained nitrogen spectra by the function ν^2 (Eq. (2)) and by the function used in the MPM (Eq. (5)) is 2 orders of magnitude less than the experimental noise throughout the studied frequency range. Therefore, in the further analysis the experimental data were approximated by the squared with frequency function.

As soon as all the values of $k(p, T)$ have been determined by optimizing the function (Eq. (2)) to the experimental spectra, the pressure dependence of the found values is modeled according to (Eq. (3)). The result of such processing is shown in Fig. 2. As expected, the pressure dependence of absorption in nitrogen is described well by a quadratic function for all experimental temperatures, which justifies interpretation of the observed spectra in terms of bimolecular absorption.

The final step is the approximation of the temperature dependence of data according to Eq. (4). The result is presented in

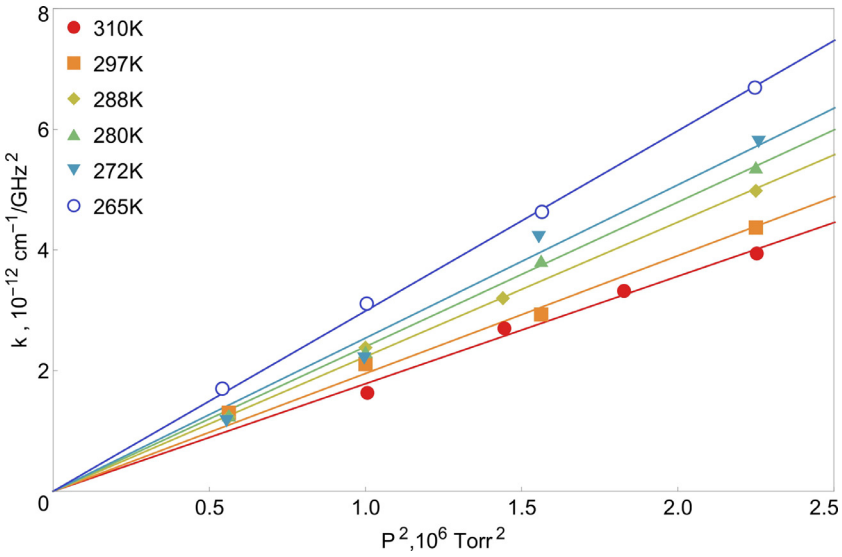

Fig. 2. Nitrogen continuum coefficient $k(p, T)$ from Eq. (3) at various experimental temperatures as a function of squared pressure. Solid lines - linear data approximation. The size of the symbols approximately corresponds to 1 σ statistical uncertainty (rms deviation).

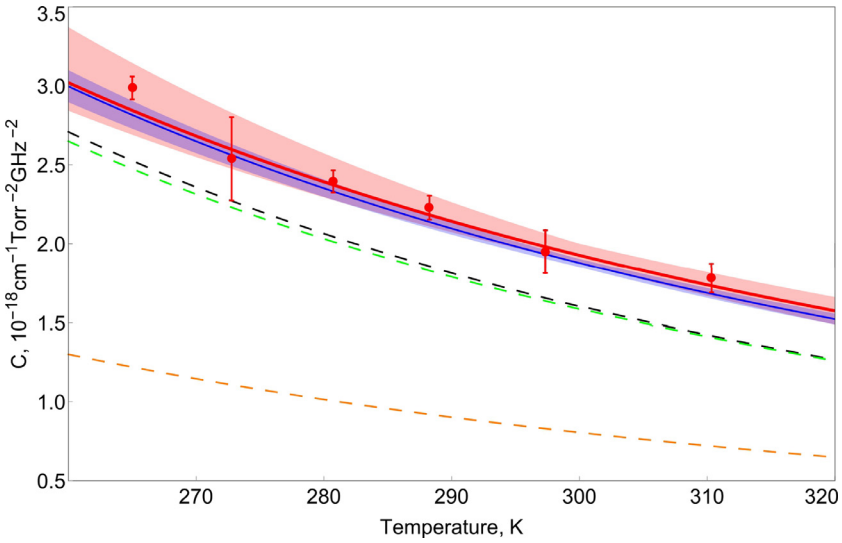

Fig. 3. Temperature dependence of nitrogen continuum coefficient. The red points stand for experimental data with 1 σ uncertainty, the solid red line shows the result of their approximation by Eq. (4); the solid blue line shows analogous dependence obtained in [10]. The filled pink and violet areas show the corresponding confidence intervals $\pm 2\sigma$. The green dashed line refers to results of the theoretical calculations by the classical trajectories method (for details see Section 4), the black dashed line shows approximation of the theoretical results [27]. The orange dashed line is approximation of the CIA temperature dependence presented in the current version of the HITRAN database [29]. All theoretical spectra were parameterized using Eqs. (1)–(4) in the frequency range 70–310 GHz and temperature interval 240–300 K. (For interpretation of the references to colour in this figure legend, the reader is referred to the web version of this article.)

Fig. 3. The following parameters were obtained: $C_0 = 1.93(5) \times 10^{-18}$ cm^{-1}/(Torr GHz)^2, $n = 3.14(30)$.

Despite the satisfactory agreement of our nitrogen absorption data with the model (Eq. (4)), we fitted the model with respect to pressure and temperature simultaneously for all the data (Fig. 4). To do so, the nitrogen absorption data for various pressures and temperatures were approximated by

$$k(p, T) = C_0 \cdot (T_0/T)^n \cdot p^2. \quad (6)$$

The values of $C_0 = 1.94(3) \times 10^{-18}$ cm^{-1}/(Torr GHz)^2 and $n = 3.27(19)$ obtained in the course of the global fit agree within the estimated error bars with the results of successive approximation mentioned above, thus validating the data treatment method.

4. Semiclassical trajectory-based simulation of the N_2–N_2 rototranslational spectra

The salient features of our semiclassical method and its application to simulation of the CIA rototranslational (RT) band in N_2–N_2 molecular pair are described in [30]. The calculations therein relied on the use of the most accurate to date *ab initio* calculated potential energy and induced dipole surfaces reported in [31]. The problem of the RT band simulation using a representative ensemble of the classical trajectories can be divided into several stages the details of each of which are stated in [30]. First, rigorous classical Hamiltonian $H(\boldsymbol{q}, \boldsymbol{p})$ was employed for two interacting rigid linear molecules using the so-called body-fixed frame of reference. Second, the initial conditions were sampled from the Boltzmann

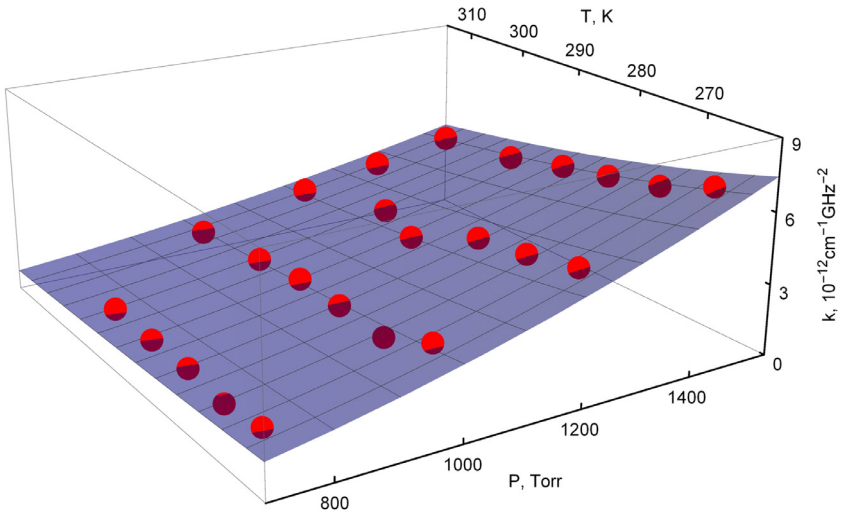

Fig. 4. The result of a simultaneous fit of Eq. (6) to the totality of experimental data. The points show the calculated values of the $k(p, T)$ coefficient (the size of the symbols approximately corresponds to 1σ statistical uncertainty), the surface shows the result of data approximation by Eq. (6).

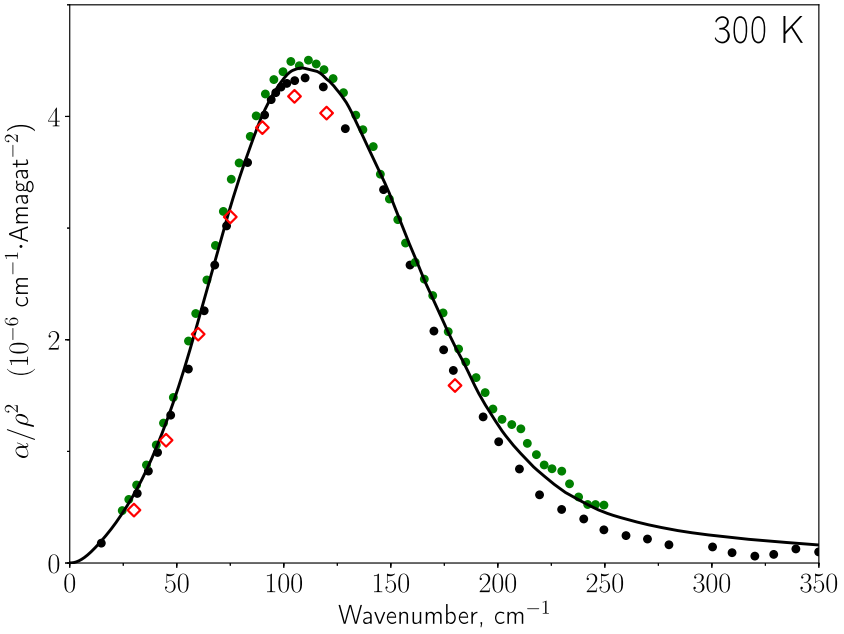

Fig. 5. N_2–N_2 collision-induced absorption spectra at room temperature. Trajectory-based profile [30] is shown by solid line. The empty red diamonds show the result of quantum mechanical calculations [31]. The black and green circles represent the data measured in [32,33], respectively. (For interpretation of the references to colour in this figure legend, the reader is referred to the web version of this article.)

distribution

$$\rho(\mathbf{q}, \mathbf{p}) = \frac{1}{Q} \exp\left(-\frac{H(\mathbf{q}, \mathbf{p})}{kT}\right)\Bigg|_{R=R_{\max}} \tag{7}$$

at fixed and large enough intermolecular separation $R_{\max}$ between molecular centers of mass. Here $\boldsymbol{q}$ and $\boldsymbol{p}$ are the vectors of generalized coordinates and conjugated momenta, respectively, and Q is the partition function

$$Q = \int \cdots \int \exp\left(-\frac{H}{kT}\right) \mathrm{d}\mathbf{q}\mathrm{d}\mathbf{p}. \tag{8}$$

The next stage is the calculation of an ensemble of classical collisional trajectories starting from the sampled initial conditions by integrating Hamilton's equations of motion. Finally, having then calculated the time-dependencies of the induced dipole $\boldsymbol{\mu}(t)$ along each of the collisional trajectories, the classical spectral density function can be found in terms of the integral [30]

$$G_{\text{class}}(\omega) = \frac{1}{2\pi Q} \int_{-\infty}^{0} \frac{-p_R}{\mu} \mathrm{d}p_R \times \int_{H>0} \cdots \int \exp\left(-\frac{H}{kT}\right) \mathrm{d}\mathbf{q}^{\star}\mathrm{d}\mathbf{p}^{\star} \left| \int_{-\infty}^{+\infty} \boldsymbol{\mu}(t) e^{-i\omega t} \mathrm{d}t \right|^2. \tag{9}$$

Here $\omega = 2\pi\nu$ is angular frequency, $\boldsymbol{q}^{\star}$ and $\boldsymbol{p}^{\star}$ denote the reduced vectors of generalized coordinates $\boldsymbol{q}$ and conjugated momenta $\boldsymbol{p}$ which are obtained from the complete set of coordinates and momenta by exclusion of the intermolecular coordinate R and the relevant p_R moment.

The $G_{\text{class}}(\omega)$ function allows determination of the absorption coefficient $\alpha_{\text{class}}(\omega)$ normalized to the density squared using the

Table 1
The first spectral moments for the N_2–N_2 system. The columns show, respectively, temperature in Kelvin, the values of spectral moments $M_0(H>0)$ and $M_2(H>0)$ arising from the phase space averaging, M_0^{traj} and M_2^{traj} from the integration of trajectory-based spectral function, and their relative difference Δ in per cent. The zeroth and second spectral moments are given in cm^{-1} Amagat^{-2} and cm^{-3} Amagat^{-2}, respectively.

T, K	$M_0(H>0)$ $M_2(H>0)$	M_0^{traj} M_2^{traj}	Δ, %
78.3	6.059×10^{-5}	6.103×10^{-5}	+0.7
	1.049×10^{-1}	1.074×10^{-1}	+2.3
89.3	5.487×10^{-5}	5.517×10^{-5}	+0.5
	1.068×10^{-1}	1.089×10^{-1}	+2.0
109.6	4.817×10^{-5}	4.865×10^{-5}	+1.0
	1.137×10^{-1}	1.156×10^{-1}	+1.7
129.0	4.444×10^{-5}	4.414×10^{-5}	−0.7
	1.227×10^{-1}	1.232×10^{-1}	+0.4
149.0	4.178×10^{-5}	4.271×10^{-5}	+2.2
	1.332×10^{-1}	1.357×10^{-1}	+1.9
179.0	3.941×10^{-5}	3.934×10^{-5}	−0.2
	1.513×10^{-1}	1.503×10^{-1}	−0.7
228.3	3.756×10^{-5}	3.768×10^{-5}	+0.3
	1.848×10^{-1}	1.859×10^{-1}	+0.6
300.0	3.650×10^{-5}	3.576×10^{-5}	−2.0
	2.389×10^{-1}	2.339×10^{-1}	−2.1
343.0	3.638×10^{-5}	3.666×10^{-5}	+0.7
	2.741×10^{-1}	2.736×10^{-1}	−0.2

conventional relationship [3]

$$\frac{\alpha_{\text{class}}(\omega)}{\rho^2} = \frac{(2\pi)^3 N_L^2 \omega}{3\hbar}\left[1-\exp\left(-\frac{\hbar\omega}{kT}\right)\right] V G_{\text{class}}(\omega), \tag{10}$$

where $\hbar$ is the reduced Planck's constant, k is the Boltzmann constant, and V is the sample volume.

The classical spectral function is known to be symmetrical [3]

$$G_{\text{class}}(\omega) = G_{\text{class}}(-\omega), \tag{11}$$

therefore it does not conform to the quantum principle of detailed balance. The *ad hoc* corrections are thus introduced for the classically calculated spectral profile. A reasonable desymmetrization procedure was chosen in [30] so that the absorption coefficient

$$\alpha(\omega) = \alpha_{\text{class}}(\omega) e^{\hbar\omega/2kT} \tag{12}$$

is considered as a semiclassically calculated trajectory-based spectral profile and compared with experimental observations. An illustrative example of the N_2–N_2 RT spectrum at room temperature (Fig. 5) was obtained as a result of the statistical average over an ensemble of two million classical trajectories. It is seen that our trajectory-based spectrum agrees well with available experimental data within the broad spectral range. Our data are close also to the results of pure quantum mechanical calculations [31] obtained at selected wavenumber points using the same as in [30] potential and induced dipole surfaces.

As a supplementary theoretical test of reliability of our calculated spectra we performed calculation of the first spectral moments. These values can be derived from two significantly different prerequisites. On the one hand, the n-th order spectral moment of the spectral function $G(\omega)$ is defined as

$$M_n = (2\pi c)^{-n-1}\int_{-\infty}^{+\infty}\omega^n V G(\omega) d\omega, \tag{13}$$

In what follows, we restrict ourselves to the first spectral moments only, i.e., to the cases $n=0$ and $n=2$. On the other hand, spectral moments can be determined as statistical averages [3]

$$M_0 = \frac{V}{4\pi\varepsilon_0}\frac{1}{2\pi c}\langle \boldsymbol{\mu}^2\rangle, \tag{14}$$

Table 2
Comparison of the experimental conditions and obtained continuum parameters.

	This work	[10]
Frequency range, GHz	105–200	170–260
Pressure range, Torr	750–1500	800–2250
Temperature range, K	265–310	230–320
Resonator length, m	0.5	10
C_0, $\text{cm}^{-1}/(\text{Torr GHz})^2$	$1.94(3)\times10^{-18}$	$1.877(13)\times10^{-18}$
n	3.27(19)	3.27(7)

$$M_2 = \frac{V}{4\pi\varepsilon_0}\frac{1}{(2\pi c)^3}\langle \dot{\boldsymbol{\mu}}^2\rangle, \tag{15}$$

where ε_0 is the vacuum permittivity and the angular brackets mean averaging over phase space.

We expect the moments calculated from the frequency range integration of the trajectory-based spectral function to be equal to the moments obtained as a result of the phase space averaging. There are, however, two important requirements for this statement to be a reality. First, both the spectral function in (13) and the spectral moments in (14) and (15) have to be calculated over the same domain in the phase space. Second, the amount of trajectories has to be sufficient to guarantee convergence of the statistical average in (9). In the calculations reported in [30], only scattering trajectories are considered that belong to the domain of the so-called free and quasi-bound N_2–N_2 pairs [5]. Consequently, to compare the moments issued from the trajectory-based spectral function in (13) with those from (14), (15) we have to restrict the domain of integration in the latter ones by exclusion of the contribution from true bound dimers, i.e. by assuming a strictly positive total Hamiltonian $H>0$. The values of our calculated spectral moments are shown in the Table 1. Fig. 6 shows the $M_0(H>0)$ and $M_2(H>0)$ temperature variations as calculated from the space phase integration in comparison with the values retrieved from the experimental spectra. Also shown are the M_0 and M_2 values calculated from trajectory-based spectral functions.

5. Discussion

Comparison of our experimental results with those from the most relevant study by Meshkov and De Lucia [10] can be made using Table 2. The value of the coefficient C_0 retrieved in our work is 3% in excess of that in [10], both values agree with each other within 2σ. A good agreement of these two experiments is demonstrated in Fig. 3, where the absorption in nitrogen is plotted as a function of temperature. The agreement within the estimated uncertainty between two independent experimental studies performed at different facilities, under different conditions and in different frequency ranges suggests that systematic errors were minimized in both experiments. This characterizes the reliability of the data obtained in both experiments, the joint frequency range of which covers a significant part of the millimeter wavelength range and allows using them for validating available models.

Fig. 3 permits also to compare our experimental results with results of available theoretical simulations. The quantum calculations performed by Borysow and Frommhold [27] were made assuming isotropic intermolecular potential as well as using semi-empirical parameters. Note that the data from [27] were used for determination of the continuum coefficients in the MPM. These data are in a nearly perfect agreement with results of our classical trajectories calculations, in which complete *ab initio* potential and dipole surface were used with no adjustable parameters. However, both theoretical models systematically underestimate experimental results by approximately 10%. Worth mentioning is that in our theoretical

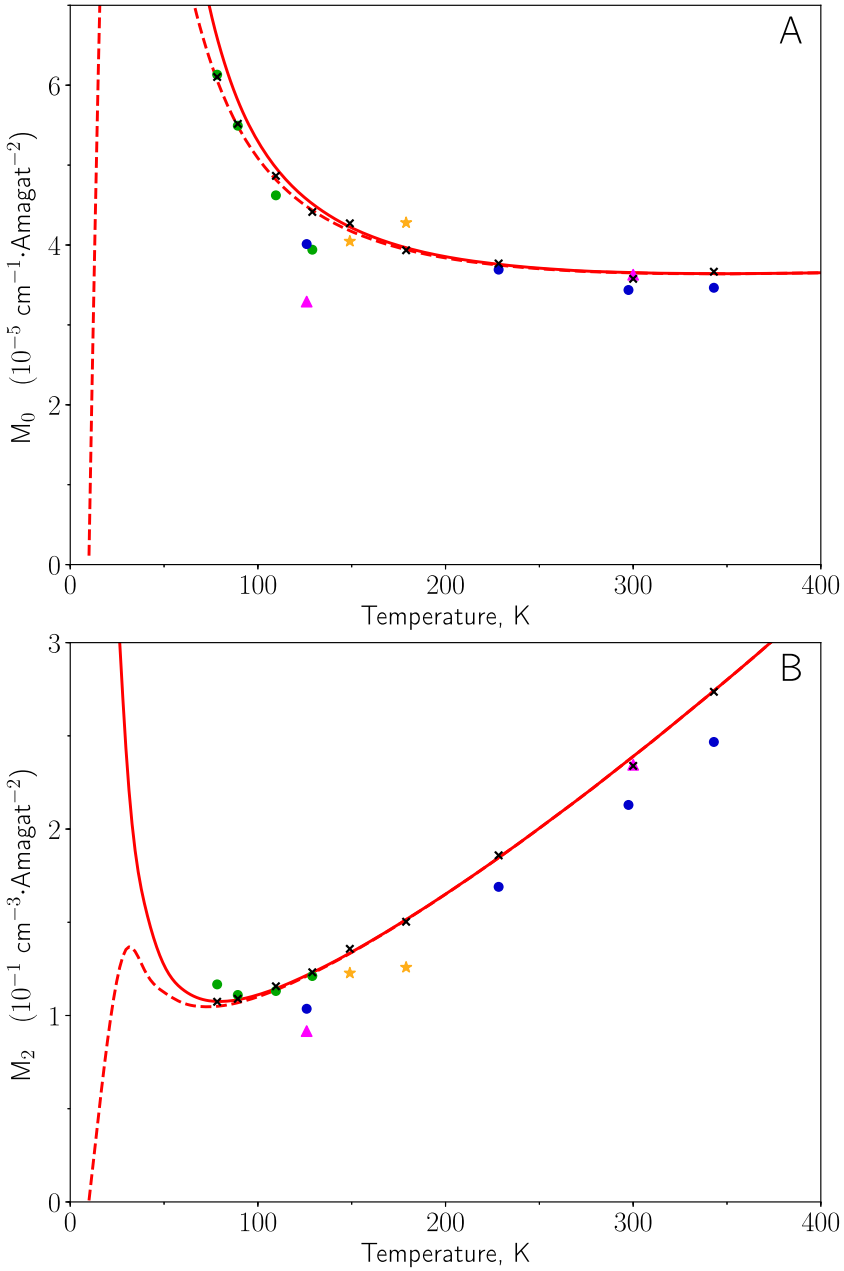

Fig. 6. Temperature dependence of the zeroth (panel A) and the second (panel B) spectral moments for the N_2–N_2 system. The solid and dashed lines, respectively, refer to spectral moments obtained by averaging over complete phase space and its domain corresponding to free and quasi-bound states. The green circles, blue circles, magenta triangles, and orange stars represent measured data from [29,32–34], respectively. The crosses show spectral moments issued from trajectory-based spectral functions. (For interpretation of the references to colour in this figure legend, the reader is referred to the web version of this article.)

simulation the contribution from true bound nitrogen dimers was completely disregarded.

The contribution from true bound states to absorption can be evaluated through analysis of the spectral moments shown in Fig. 6. Negligible contribution from true bound dimers to integrated characteristics of the absorption is clearly seen within the whole range of atmospheric temperatures. In the vicinity of room temperature true bound states are responsible for about 0.1% and 0.008% contribution to the zeroth and the second spectral moments, respectively. It is therefore unlikely to expect that the contribution from true bound $(N_2)_2$ dimers is capable to fill the observed gap (Fig. 3) between the trajectory-based absorption coefficient and the experimental values measured in the present work irrespective of how the associated dimer absorption spectral profile may look like. In other words, the true dimer absorption can hardly give rise to a noticeable change in the N_2–N_2 CIA reported as a result of trajectory-based calculations at least within the range of typical atmospheric conditions.

Both theoretical calculations do not take into account the contribution from regular rotational lines of N_2 monomer related to quadruple transitions and to dipole transitions of asymmetric molecular isotopologue $^{14}N^{15}N$ contained in experimental spectra. This absorption is, however, a few orders of magnitude smaller than bimolecular absorption, as can be easily evaluated using the related data from HITRAN [35].

Another potential source of the difference is experimental overestimation of the N_2–N_2 absorption. The systematic uncertainty of C_0 parameter which can be caused by the uncertainties of

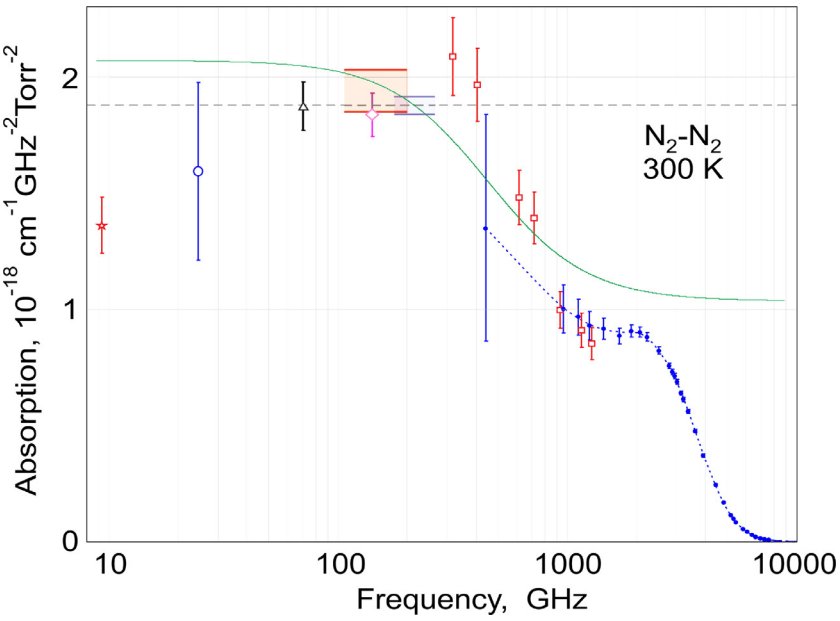

Fig. 7. The nitrogen continuum absorption at 300 K normalized by pressure and frequency squared. Experimental results of the present work are shown by pink rectangle, experimental results of the work [10] are shown by blue rectangle. The vertical sizes of the rectangles corresponds to the experimental uncertainties. Black dashed line is the ν^2 approximation of data from [10]. Green line is the MPM-based model (Eq. (5)) fitted to the joint quasi-experimental data (see the text). Experimental results from the other works are shown by symbols: red star - [37], blue circle - [38], black triangle - [39], pink diamond - [9], red squares - [40], blue points - [32]. Blue dotted line is the smooth interpolation of the experimental points from [32]. (For interpretation of the references to colour in this figure legend, the reader is referred to the web version of this article.)

pressure and temperature sensors is about 0.6% which is negligible in comparison with the difference. One more probable reason for such overestimation is related to water molecules, which are permanently present as minor impurity in the gas sample or in spectrometer chamber. Maximal possible water vapor content can be evaluated from the spectrum recording shown in Fig. 1. The water vapor line near 183 GHz with integrated intensity of 8.16×10^{-23} cm/molec at $T = 288.3$ K (for comparison see, e.g., Fig. 4 from [36]) is not seen, therefore the relevant absorption at the line maximum is smaller than standard deviation of experimental noise. The upper limit for the partial water vapor pressure in this case is 3.6 mTorr. The corresponding water vapor contribution to the total observed absorption can be up to about 2%. This potential error is smaller than statistical uncertainty of measurements and can be neglected. Moreover, this potential extra absorption is mostly determined by H_2O–N_2 foreign continuum. It scales linearly with nitrogen pressure and thus would manifest itself as slight deviation from the observed quadratic dependence (Fig. 2). Note that similar conclusions about the potential impact of water vapor on the result of measurements were made in [10].

All these considerations mean that the nature of the slight deviation between experimental data and our trajectory-based prediction in Fig. 3 remains undetermined.

Fig. 3 presents also relevant data for N_2–N_2 absorption from the current version of HITRAN/CIA database. These data are significantly (several times) lower than experimental data. The N_2–N_2 data included in HITRAN CIA for microwave spectral range rely on the results of recent quantum calculations by Karman et al. [31], in which, in contrast to [27], the complete anisotropic intermolecular potential was used. Generally, the results obtained in [31] are in a good agreement with the results of [27], at least near the maximum of the RT band, though the absorption on a rare frequency grid was only calculated in [31]. The frequency range considered in our work is far beyond the spectral points at which quantum calculations were made. We believe therefore that the significant discrepancy between the experimental data and the values collected for the spectral range in question in [29] might be caused simply by non-optimal choice of interpolating function.

In order to compare the absorption determined in [10] and in the present work with that given by the MPM model (Eq. (5)), we have calculated the absorption normalized to the pressure squared using Eqs. (2)–(4) with a frequency step of 250 MHz for which the coefficients C and n were borrowed from Table 2. Two spectra were calculated for selected temperatures: 265.0, 272.8, 280.7, 288.3, 297.3 and 310.3 K. First, within the frequency range of this work and making use of the coefficients obtained by us and, second, within the 170–260 GHz frequency range with the use of the coefficients obtained in [10]. For the temperatures of 228.8, 251.6, 261.9, 313.8, and 323.1 K at which the measurements were performed in [10], only one spectrum was calculated in the 170–260 GHz range using the coefficients from [10]. The uncertainty of the calculated absorption coefficients was determined by statistical uncertainty of the continuum coefficients (Table 2). As a result of the joint approximation of the entire set of such "quasi-experimental" data, using model (Eq. (5)) we obtained new nitrogen continuum coefficients $C_{M_{new}} = 2.066 \times 10^{-18}$ cm^{-1}/(Torr GHz)^2 and $n_{new} = 3.27$. Fig. 7 demonstrates these quasi-experimental data for 300 K as well as the result of their approximation by the model (Eq. (5)). Under these conditions, the coefficient $C_M = 1.85 \times 10^{-18}$ cm^{-1}/(Torr GHz)^2 used in the modern version of MPM [15] underestimates the value of the experimentally determined absorption by approximately 10%. For comparison, Fig. 7 shows the absorption calculated for the same conditions based on the data available from other works. One can see that experimental data within the millimeter spectral range can be described better by the quadratic frequency dependence (dashed line in Fig. 7) than by the model (Eq. (5)). However, in the range extended to 300 GHz, the difference between these two models (Eqs. (2) and (5)) is of the order of experimental uncertainty. The model function (Eq. (5)) is more justified from the point of view of the physical features of the spectrum and corresponds better to the absorption in the submillimeter range. That is why we rec-

ommend to use it in propagation models together with the coefficients refined in this paper until a more accurate and theoretically well grounded model will be suggested.

Conclusion

Continuum absorption in nitrogen was remeasured using the highly sensitive resonator spectrometer within the 105–200 GHz spectral range at temperatures and pressures typical for the Earths atmosphere. The frequency dependence of the absorption was analysed and the power exponent of its temperature dependence was determined. The results obtained were compared with the data of the previous studies and with the theoretical calculations based on analysis of the classical scattering trajectories. The set of refined continuum parameters was derived, the use of which can be recommended to increase accuracy of the radiation propagation models in the atmosphere.

Declaration of competing interest

The author declare that they have no known competing financial interests or personal relationships that could have appeared to influence the work reported in this paper.

CRediT authorship contribution statement

E.A. Serov: Investigation, Project administration, Writing - review & editing. **A.A. Balashov:** Investigation, Writing - original draft, Visualization. **M.Yu. Tretyakov:** Conceptualization, Methodology, Writing - review & editing. **T.A. Odintsova:** Investigation, Validation, Formal analysis. **M.A. Koshelev:** Methodology, Investigation, Validation. **D.N. Chistikov:** Methodology, Software. **A.A. Finenko:** Methodology, Software. **S.E. Lokshtanov:** Methodology. **S.V. Petrov:** Methodology. **A.A. Vigasin:** Methodology, Writing - original draft, Supervision.

Acknowledgements

The experimental studies and data analysis were supported by the Russian Foundation for Basic Research, Grants 18-05-00698 and 18-05-00119. Partial support of this work from The Ministry of Science and Higher Education of the Russian Federation, Project 19-270 and from Presidium of RAS Program 5 is gratefully acknowledged.

References

[1] Becker GE, Autler SH. Water vapor absorption of electromagnetic radiation in the centimeter wave-length range. Phys Rev 1946;70:300–7.
[2] Van Vleck JH, Weisskopf VF. On the shape of collision-broadened lines. Rev Mod Phys 1945;17:227–36.
[3] Frommhold L. Collision-induced absorption in gases. Cambridge University Press; 2006.
[4] Vigasin AA. Water vapor continuum: whether collision-induced absorption is involved? J Quant Spectrosc Radiat Transf 2014;148:58–64.
[5] Vigasin AA. In: weakly interacting molecular pairs: unconventional absorbers of radiation in the atmosphere. Dordrecht: Springer; 2003. 23–47
[6] http://weather.uwyo.edu/upperair/sounding.html.
[7] Maryott AA, Birnbaum GB. Microwave absorption in compressed oxygen. Phys Rev 1955;99. 1886
[8] Strandberg MWP, Meng CY, Ingersoll JG. The microwave absorption spectrum of oxygen. Phys Rev 1949;75:1524–8.
[9] Dagg IR, Reesor GE, Wong M. A microwave cavity measurement of collision-induced absorption in n_2 and CO_2 at 4.6 cm^{-1}. Can J Phys 1978;56:1037–45.
[10] Meshkov AI, De Lucia FC. Laboratory measurements of dry air atmospheric absorption with a millimeter wave cavity ringdown spectrometer. J Quant Spectrosc Radiat Transf 2007;108:256–76.
[11] Liebe HJ. The atmospheric water continuum below 300 GHz. Int J Infrared Millimeter Waves 1984;5:207–27.
[12] Liebe HJ. An updated model for millimeter wave propagation in moist air. Radio Sci 1985;20:1069–89.
[13] Liebe HJ. MPM-an atmospheric millimeter-wave propagation model. Int J Infrared Millimeter Waves 1989;10:631–50.
[14] Rosenkranz PW. Water vapor microwave continuum absorption: a comparison of measurements and models. Radio Sci 1998;33:919–28.
[15] Rosenkranz PW. Remote sens. Code Libr 2017. doi:10.21982/M81013.
[16] Read WG, Waters JW, Wu DL, Stone EM, Shippony Z, Smedley AC, et al. UARS microwave limb sounder upper tropospheric humidity measurements: method and validation. J Geophys Res 2001;106:32207–58.
[17] Cimini D, Rosenkranz PW, Tretyakov MY, Koshelev MA, Romano F. Uncertainty of atmospheric microwave absorption model: impact on ground-based radiometer simulations and retrievals. Atmos Chem Phys 2018;18:15231–59. doi:10.5194/acp-18-15231-2018.
[18] Santee ML, Manney GL, Livesey NJ, Froidevaux L, Schwartz MJ, Read WG. Trace gas evolution in the lowermost stratosphere from Aura Microwave Limb Sounder measurements. J Geophys Res 2011;116:D18306. doi:10.1029/2011JD015590.
[19] Maschwitz G, LÀ¶ hnert U, Crewell S, Rose T, Turner DD. Investigation of ground-based microwave radiometer calibration techniques at 530 hPa. Atmos Meas Tech 2013;6:2641–58. doi:10.5194/amt-6-2641-2013.
[20] Cimini D, Westwater ER, Gasiewski AJ. Temperature and humidity profiling in the arctic using ground-based millimeter-wave radiometry and 1DVAR. IEEE Trans Geosci Remote Sens 2010;48:1381–8.
[21] Gamache RR, Hartmann JM. An intercomparison of measured pressure-broadening and pressure-shifting parameters of water vapor. Can J Chem 2004;82:1013–27.
[22] Payan S, La D, Noe J, Hauchecorne A, Camy-Peyret C. A review of remote sensing techniques and related spectroscopy problems. CR Phys 2005;6:825–35.
[23] Courtin R. Pressure-induced absorption coefficients for radiative transfer calculations in Titan's atmosphere. ICARUS 1988;75:245–54. doi:10.1016/0019-1035(88)90004-8.
[24] Krupnov AF, Tretyakov MY, Parshin VV, Shanin VN, Myasnikova SE. Modern millimeter-wave resonator spectroscopy of broad lines. J Mol Spectrosc 2000;202:107–15.
[25] Koshelev MA, Leonov II, Serov EA, Chernova AI, Balashov AA, Bubnov GM, Andriyanov AF, Shkaev AP, Parshin VV, Krupnov AF, Tretyakov MY. New frontiers in modern resonator spectroscopy. IEEE Trans Terahertz Sci Technol 2018;8:773–83. doi:10.1109/TTHZ.2018.2875450.
[26] Serov EA, Parshin VV, Bubnov GM. Reflectivity of metals in the millimeter wavelength range at cryogenic temperatures. IEEE Trans Microw Theory Tech 2016;64:3828–38.
[27] Borysow A, Frommhold L. Collision-induced rototranslational absorption spectra of N_2-N_2 pairs for temperatures from 50 to 300 K. Astrophys J 1986;311:1043. doi:10.1086/164841.
[28] Boissoles J, Boulet C, Tipping RH, Brown A, Ma Q. Theoretical calculation of the translation-rotation collision-induced absorption in N_2–N_2 , O_2–O_2, and N_2–O_2 pairs. J Quant Spectrosc Radiat Transf 2003;82:505–16.
[29] Karman T, Gordon IE, van der Avoird A, Baranov YI, Boulet C, Drouin BJ, Groenenboom GC, Gustafsson M, Hartmann J-M, Kurucz RL, Rothman LS, Sun K, Sung K, Thalman R, Tran H, Wishnow EH, Wordsworth R, Vigasin AA, Volkamer R, van der Z, J W. Update of the HITRAN collision-induced absorption section. ICARUS 2019;328:160–75.
[30] Chistikov DN, Finenko AA, Lokshtanov SE, Petrov SV, Vigasin AA. Simulation of collision-induced absorption spectra based on classical trajectories and *ab initio* potential and induced dipole surfaces. I Case study of N_2–N_2 rototranslational band. J Chem Phys 2019;151:194106. doi:10.1063/1.5125756.
[31] Karman T, Miliordos E, Hunt KLC, Groenenboom GC, van der AA. Quantum mechanical calculation of the collision-induced absorption spectra of N_2-N_2 with anisotropic interactions. J Chem Phys 2015;142:084306. doi:10.1063/1.4907917.
[32] Stone NWB, Read LAA, Anderson A, Dagg IR, Smith W. Temperature dependent collision-induced absorption in nitrogen. Can J Phys 1984;62:338–47.
[33] Buontempo U, Cunsolo S, Jacucci G, Weis JJ. The far infrared absorption spectrum of N_2 in the gas and liquid phases. J Chem Phys 1975;63:2570–6.
[34] Dagg IR, Anderson A, Yan S, Smith W, Read LAA. Collision-induced absorption in nitrogen at low temperatures. Can J Phys 1985;63:625–31.
[35] Gordon IE, Rothman LS, Hill C, Kochanov RV, Tan Y. The HITRAN2016 molecular spectroscopic database. J Quant Spectr Radiat Transf 2017;203:3–69. doi:10.1016/j.jqsrt.2017.06.038.
[36] Tretyakov MY. Spectroscopy underlying microwave remote sensing of atmospheric water vapor. J Mol Spectrosc 2016;328:7–26.
[37] Ho W, Kaufman IA, Thaddeus P. Pressure-induced microwave absorption in N_2. J Chem Phys 1968;49:3627–31.
[38] Birnbaum G, Maryott AA. Collision-induced microwave absorption in compressed gases. II. Molecular electric quadrupole moments. J Chem Phys 1962;36:2032–6.
[39] Dagg IR, Reesor GE, Urbaniak JL. Collision induced absorption in N_2, CO_2, and H_2 at 2.3 cm^{-1}. Can J Phys 1975;53:1764–76.
[40] Occelli R, Chaaban H, Moynault JM, Coulon R, Balsamo A. Submillimetric and millimetric collision-induced absorption spectra in compressed gaseous nitrogen using very low-frequency optical source. Can J Phys 1991;69:1264–72.